Energy 36 (2011) 4055–4062

Contents lists available at ScienceDirect

Energy

journal homepage: www.elsevier.com/locate/energy

Cloud classification in a mediterranean location using radiation data and sky images

M. Martínez-Chico [a], F.J. Batlles [b,c,*], J.L. Bosch [b]

[a] Departamento Didáctica de la Matemática y de las Ciencias Experimentales, Universidad de Almería, 04120 Almería, Spain
[b] Departamento Física Aplicada, Universidad de Almería, 04120 Almería, Spain
[c] CIESOL, Universidad de Almería, 04120 Almería, Spain

ARTICLE INFO

Article history:
Received 29 October 2010
Received in revised form
25 April 2011
Accepted 26 April 2011
Available online 8 June 2011

Keywords:
Cloud characterisation
Beam transmittance
Total sky imager
Direct solar radiation attenuation

ABSTRACT

Knowledge regarding the solar radiation reaching the earth's surface and its geographical distribution is very important for the use of solar energy as a resource to produce electricity. Therefore, a proper assessment of available solar resource is particularly important to determine the placement and operation of solar thermal power plants. To perform this analysis correctly, it is necessary to determine the main factors influencing the radiation reaching the earth's surface, such as the earth's geometry, terrain, and atmospheric attenuation by gases, particles and clouds. Among these factors, it is important to emphasise the role of clouds as the main attenuating factor of radiation. Information about the amount and type of clouds present in the sky is therefore necessary to analyse both their attenuation levels and the prevalence of different sky conditions. Cloud cover is characterised according to attenuation levels, using the beam transmittance (k_b, ratio of direct radiation incident on the surface to the extraterrestrial solar radiation) and hemispherical sky images. An analysis of the frequency and duration of each type of cloud cover blocking the sun's disk is also performed. Results show prevailing sky situations that make the studied area very suitable for the use of solar energy systems.

1. Introduction

Increasing demand for electricity, coupled with a declining fossil fuel base and the consequences of greenhouse gas emissions, have stimulated efforts worldwide for developing cheap and reliable supplies of electricity from renewable sources. This is why power production using solar energy has improved globally, experiencing a significant expansion that primarily reduces costs and achieves greater conversion efficiency. In the last decade, solar thermal power plant development has been used as an alternative to fossil fuels. By concentrating solar radiation from heliostats, thermal fluid can reach very high temperatures; the resulting heat is converted to kinetic energy in a steam cycle that generates electricity with either turbine generators or heat exchangers.

One of the most important steps when using any renewable energy is to obtain an accurate estimation of the resource that must be exploited. In this respect, specific knowledge of direct radiation and its attenuation is essential for devices that concentrate solar radiation, as is the case of solar power towers. This is due to the fact that direct radiation incidence angle is always known, so optical concentration systems can be designed to focus this component of solar radiation.

The sun is an unfailing, but intermittent, source of energy. There are strong daily and seasonal variations resulting in great fluctuations of the solar resource availability. This availability is also limited by cloud cover. To extend power generation beyond periods of sunlight and allow a constant heat supply, solar thermal energy storage plants have been developed. Nevertheless, the main problem for these systems occurs when the sun is interrupted for short periods (e.g., due to clouds). During normal operating conditions, the mean temperature of the receiver is stabilised. However, when the sun is covered by clouds, a sudden reduction in solar radiation occurs, followed by a rapid decrease of the receiver temperature, because of the relatively low thermal inertia of the receiver (its outlet power or temperature or both change quickly) [1]. The opposite result occurs when the clouds stop blocking the sun with the consequent increase of the receiver temperature. These rapid changes in temperature can lead to thermal stress, and if this phenomenon occurs several times, the receiver may break [2]. As a result, one of the main problems in the operation of solar power tower plants is to predict when a cloud will cover the area of interest and the level of solar radiation attenuation. The study of cloud cover is therefore especially important due to the

* Corresponding author. Departamento Física Aplicada, Universidad de Almería, 04120 Almería, Spain, Tel.: +34 950 015914; fax: +34 950 015477.
E-mail address: fbatlles@ual.es (F.J. Batlles).

0360-5442/$ – see front matter © 2011 Elsevier Ltd. All rights reserved.
doi:10.1016/j.energy.2011.04.043

outstanding role of clouds as the main attenuators of solar radiation in the atmosphere, and because their high spatial and temporal variability.

In the last decades, this study has been addressed using different methods and data of different types. Historically, cloud measurements from the surface were accomplished by human observations, annotating the amount of clouds covering the sky (octas) and distinguishing the types of clouds according to their appearance, but this data collection was expensive and subjective. Such measurements are still used [3] when performing long-term evaluations when no other data are available, i.e. Sabziparvara and Shetaeeb [4] obtained good results using the cloud fraction to forecast solar radiant energy in arid and semi-arid regions. More recently, however, these human-based observations of cloud cover have been used to supplement cloud estimations by newer techniques and to verify the accuracy of results [5,6].

More recently, other techniques have been employed for the detection of cloudiness. For example, an Automatic Partial Cloud Amount Detection Algorithm (APCADA) has been developed [6] for estimating the actual sky cloud cover (high clouds cannot be detected by this method due to their thinness) from surface measurements of long-wave downward radiation, temperature, and relative humidity taken every 10 min. Some authors [7] have estimated partial cloud amounts according to the above algorithm. They have validated their results against both human observations and digital all-sky images to establish the APCADA scheme at a coastal site for long-term observations of cloud cover and to quantify errors resulting from the different detection methods.

Cloud cover has also been studied using satellite images [8–12]. Zarzalejo et al. [8] developed an artificial intelligence-based model to estimate the influence of satellite-detected clouds on the hourly solar irradiation reaching the surface. Bosch et al. [9] used a satellite-derived cloud index to evaluate the influence of both cloud cover and topography on solar resources. Derrien et al. [10] performed cloud detection through a real-time processing scheme based upon threshold tests applied to different combinations of the spectral irradiances measured by the NOAA-11 satellite. Cloud edges and subpixel clouds were detected over continental surfaces with a special test. Furthermore, Perez et al. [11] estimated solar radiation by means of a model using satellite visible images and considering the apparent cloud cover. Mefti et al. [12] generated hourly global solar irradiation data using a satellite-based model that showed systematic improvement in the performance of the tested locations.

Some studies focused on the influence of cloud cover on UV radiation [13–15]. Alados-Arboledas et al. [14] observed that the attenuation of UVB radiation by clouds is frequently larger than the attenuation produced by any other atmospheric parameter. In addition, an empirical parameter called the "cloud modification factor" was used in [13,15], that is generally defined as the ratio of radiation from an overcast sky to the radiation from a clear sky.

In the last decade, the study of cloud cover has been addressed using all-sky imagers [16–19]. For example, Pfister et al. [16] compared the results from two of these imagers to quantify the reproducibility of an automated detection technique. Furthermore, Sabburg and Long [17] asserted that the use of all-sky imaging systems offers the ability to understand and quantify cloud effects more accurately. Moreover, Kassianov et al. [18] attempted to improve the use of these devices by creating a method to convert surface measurements of sky cover determined from images taken with a TSI-880 (Total Sky Imager-880, Yankee Environmental Systems Inc.). Their aim was to vertically project the cloud fraction and examine the relationship between hemispherical sky cover and the nadir-view cloud fraction. A more recent paper by Long et al. [19] characterised clouds from colour all sky images taken from the earth's surface during daytime. The authors described two types of sky imaging systems and compared processing methods for cloud cover detection with human observations and the visual analysis of sky images.

Although clouds generally reduce the solar radiation reaching the surface of the earth, there are particular situations in which they can cause higher radiation levels than those expected for a cloudless sky. In these cases, instantaneous values of global radiation close to the solar constant (I_{sc}, irradiance received per unit area at the top of the atmosphere, perpendicular to the propagation direction and equal to 1367 W/m^2) were found. This effect, caused by certain clouds, has been studied by many authors [15,16,20] and is referred to as *cloud enhancement*; it occurs when the sun is not hidden, hence the entire direct solar beam reaches the surface. In addition, cloud edges near the solar disk reflect a great amount of solar radiation, which increases the value of global radiation reaching the surface. Although this is not significant at intervals longer than several minutes, incremental changes in radiation values can be important in terms of the thermal stress produced on the receiver located in the tower.

In this paper, a classification of different sky conditions has been made, considering the attenuation of direct solar radiation. This attenuation has been quantified according to the dimensionless index k_b calculated from radiation data. Furthermore, images from a total sky imager have been used to characterise the situations associated with the different values of k_b. Cloud cover in Almería has also been analysed to make a proper assessment of the solar radiation resources, and to determine an adequate operation of power generation systems in this area. To this end, the different attenuation events have been studied in terms of their duration and frequency, both for a yearly and a seasonal basis. The results of this study could be used as inputs in a variety of applications of solar radiation, such as: low-temperature solar thermal collectors, concentrated solar power plant using parabolic trough design, power towers, passive solar building design, etc. Obtained information in the regard of duration and frequency of attenuation episodes can be used in the designing and sizing of the storage systems. Cloud cover information could be also included in studies dealing with the harmful effects of UV radiation in health, because of the importance of cloud effects on UV radiation reaching the surface.

2. Data

In this section, the radiation data and sky images used in this study are described. Both types of data were recorded at a radiometric station located at the University of Almería. This site is located on the Mediterranean coast at the south-eastern end of the Iberian Peninsula. The site is affected by a mountainous ridge that blocks Atlantic maritime weather. Furthermore, Almería is one of the most arid and dry Mediterranean provinces, characterised by low annual rainfall with great seasonal irregularity. It has high insolation levels, with an annual average of more than 3000 daylight hours, which makes it particularly suitable for radiometric studies and development of solar energy technologies. Table 1 shows the different variables measured, including the sampling frequencies and the period considered.

Radiometric data used in this study was acquired at the Almería radiometric station (36.83° N, 2.41° W, 15 m m.a.s.l.), Spain, with sampling frequency of 1 min. Horizontal solar global and diffuse radiation was measured by two Kipp & Zonen CM-11 pyranometers, while direct solar radiation was acquired with a Kipp & Zonen CH1 pyrheliometer. Both were anchored to a 2*AP* two-axis solar tracker (Kipp & Zonen). The data acquisition system consisted of a Compact Field Point with 16-bit resolution. Measurements were collected

Table 1
Characteristics of the measured variables.

Data	Frequency Measurement	Instrument	Unit	Time period
Solar global horizontal irradiance	1 min	CM-11	W/m^2	01/08/2009–31/07/2010
Solar diffuse horizontal irradiance	1 min	CM-11	W/m^2	01/08/2009–31/07/2010
Solar direct normal irradiance	1 min	CH1	W/m^2	01/08/2009–31/07/2010
Hemispherical sky image	1 min	TSI-880	–	01/08/2009–31/07/2010

between August 2009 and July 2010. The period covered by the dataset guaranteed that a complete range of seasonal conditions and solar angles were included in the samples taken.

The sampling period was set to 1 min to detect fast changes in cloud cover, which is more accurate than using average values [21]. Furthermore, solar radiation is strongly influenced by clouds, and an appropriate treatment of this influence may allow a better estimation of solar irradiation. As such, 96,319 images were analysed, covering a time period concurrent with the radiation data. The colour images had a resolution of 352 × 288 pixels and were stored in JPEG format. These images were taken with the automatic, full-colour sky imager system TSI-880, that provided a real-time display of daytime sky conditions with a hemispherical field of view. This device consisted of a Charge-Coupled Device (CCD) camera that captured a hemispherical mirror equipped with automatic rotation, which also had a "shadow band" attached to prevent damage to the optical components of the camera.

Both images and radiometric data were collected for solar elevations greater than 10°. This was done to avoid cosine response errors and because the production in solar thermal plants is minimal when the sun is near the horizon.

The radiometer domes and the mirror of the TSI-880 were cleaned on a daily basis. In addition, the solar tracker was checked daily to ensure proper tracking of the solar path. The calibration constants of the pyranometers were checked yearly. The radiation quality-control processing applied was the following: check and discard missing or negative values of solar radiation, check and discard solar global or direct solar radiation values higher than solar constant, check and discard diffuse solar radiation higher than global radiation. In addition, data loggers were synchronised (Universal Time Coordinated) to achieve a homogenous database.

3. Methodology

This section describes the methodology used for classifying and analysing the different types of clouds and their attenuation caused to direct sunlight.

3.1. Processing of radiometric data

Typically, effects of cloud cover were characterised by using global radiation measurements and dimensionless indices [22,23] (i.e., the hourly 'diffuse fraction', k, defined as the ratio of diffuse irradiance to global irradiance, and the hourly 'clearness index', k_t, defined as the ratio of global irradiance to the extraterrestrial irradiance). High k_t values were associated with clear skies, whereas low ones with overcast skies. Furthermore, in situations where the k value was low, the atmosphere had low turbidity. If we combined both indices, two different situations arose: high k_t and low k values, assigned to clear skies and low turbidity, and low k_t and high k values, associated with overcast skies and high turbidity. Other authors [24] classify the sky types analysing the illuminance distribution over the sky dome. In our study, the cloud cover was characterised according to the levels of the direct solar radiation attenuation. For this characterisation, the beam transmittance index k_b was used. This index is calculated as the ratio of direct solar radiation (B_n, the sun's direct beam arriving at the earth's surface, measured on a plane perpendicular to the beam using a collimator tube) to the extraterrestrial radiation (I_{0n}). The extraterrestrial radiation is calculated from Eq. (2), where I_{sc} is the *solar constant*, and E_0 is the *eccentricity* (a parameter that considers sun-earth distance in the year). Additionally, high k_b values were associated with clear sky conditions, whereas low values of k_b might have been due to either overcast skies or scattering caused by aerosols. The k_b index can be calculated utilising Eq. (1) and Eq. (2):

$$k_b = B_n / I_{0n} \tag{1}$$

where

$$I_{0n} = I_{sc} \cdot E_0 \tag{2}$$

This calculation was performed over the whole radiation database, and then, all the TSI images were classified according to the resulting k_b values at the moment of their capture. When all pictures were arranged in these groups, direct solar radiation values were analysed, and the images were visually checked to locate and separate situations in which no clouds blocked the sun (including both clear skies and partly cloudy skies without a shaded sun position). After the classification, the whole set of images was analysed to extract the most representative features observed for each group.

3.2. Image classification

Clouds are usually classified by means of their base height, and they are named using Latin terms to describe their appearances as seen by an observer on the ground. In this paper, cloud cover has been classified and analysed by the different levels of attenuation of the direct solar radiation reaching the surface, given by k_b, which may be more useful for energy production systems management. The classification process was:

a) For a given minute, direct solar radiation measured is used to calculate the k_b index.
b) The all-sky image captured in that minute is classified in a group depending on the k_b value
c) Images were also checked to create an additional set of cloudless sky situations.

Table 2 shows the k_b thresholds selected for performing this classification.

We grouped all images corresponding to k_b values greater than 0.6 in a single set because no situations with k_b values higher than 0.8 had been reported, as these values would imply that there was

Table 2
k_b threshold values considered and their corresponding Attenuation Groups.

Attenuation Group	k_b value
G1	$k_b < 0.2$
G2	$0.2 < k_b < 0.4$
G3	$0.4 < k_b < 0.6$
G4	$k_b > 0.6$

no atmosphere. The 96,319 images were then classified using the thresholds shown in Table 2. A subsequent review was made to group those images where the sun was not covered by clouds in a fifth set. The next step was to extract the most common features of each group that could be detected in the images. Finally, two frequency analyses were conducted. On the one hand, the occurrence of each sky condition was examined both along the entire study period and seasonally (i.e. the absolute percentage of the different attenuations groups). On the other hand, the duration of the different attenuation episodes was analysed, performing another frequency study for the durations set (i.e. the occurrence of long and short duration situations for the different attenuation groups).

4. Results and discussion

In this section, the main results of the classification and analyses described in Section 3.2 are shown, and the achieved characterisation of cloud cover of the studied area is reported.

4.1. Image classification

This section describes the most representative characteristics of clouds belonging to each attenuation group. These features include the form, colour, size, opacity, edges and type of clouds. Fig. 1(A–H) shows two different samples for each of the attenuation groups considered.

Different attenuations produced in direct solar radiation are shown in Fig. 2(A–D). These graphs correspond to the day of acquisition of some of the images in Fig. 1 and they display the direct solar radiation over the course of the day. The arrows in Fig. 2A and B point to the capture instant of the images shown in Fig. 1A and C, respectively. Ellipses in Fig. 2C and D indicates the time lapse where the solar radiation attenuation or enhancement remains (they also include the capture instant of the images shown in Fig. 1E and H, respectively).

4.1.1. Attenuation group 1, G1 ($k_b < 0.2$)

The attenuation produced in direct solar radiation by *G*1 clouds (low-level and mid-level clouds) was over 80% and was mainly due to the presence of very opaque clouds blocking the sun's disk. Interestingly, we found that such levels of attenuation were caused by clouds with several different features.

There were different situations where the sky was completely covered. The first example was very common and consisted of altostratus (As) with a uniform and homogenous base, which was also hazy and slightly blue (Fig. 1A). Another situation that could also occur is with the presence of nimbostratus (Ns) shown in Fig. 1B, characterised by a dark greygrey base. These clouds were very opaque, and their bases were dimmed by precipitation. Generally, these Ns covered large areas of sky, and their bases were heterogeneous in appearance with colours ranging from white to dark gray.

Often, there may be situations in which the sky is not completely covered, but some clouds could eventually block the sun's disk and cause strong direct solar radiation attenuation, albeit of shorter duration. These clouds can be described as "cotton-like" in appearance and may appear alone, in lines, or in clusters, but they always appear with clearly defined edges.

The strong attenuation that *G*1 clouds caused in the direct solar normal radiation can clearly be seen in Fig. 2A. At times close to solar noon, the direct solar radiation reaching the surface was negligible or nil. This situation continued until almost the end of the day, the same period of time that the clouds covered the sky.

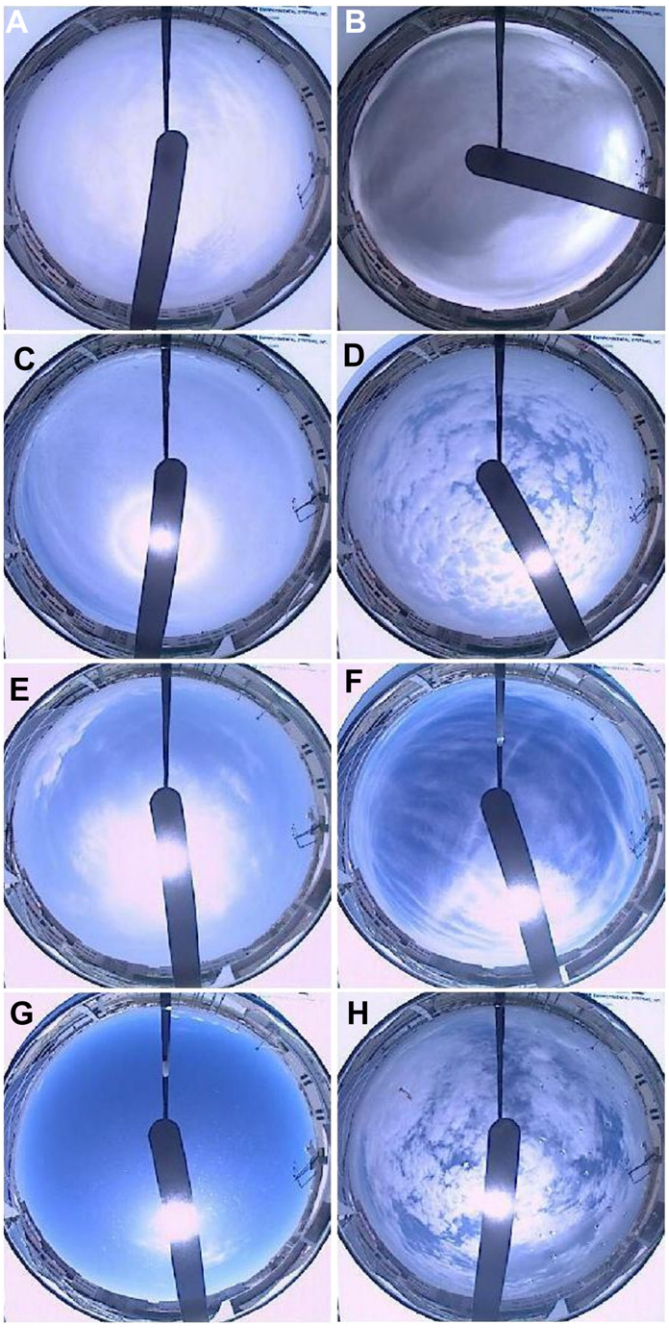

Fig. 1. Different attenuation conditions: (1A) 2010/01/19 12:50 UTC; (1B) 2010/04/05 08:25 UTC; (1C) 2010/04/22 12:18 UTC; (1D) 2010/03/14 11:06 UTC; (1E) 2009/08/03 12:08 UTC; (1F) 2010/02/27 11:33 UTC. 1(G) 2009/09/19 11:38 UTC. (1H) 2010/04/17 12:18 UTC.

4.1.2. Attenuation group 2, G2 ($0.2 < k_b < 0.4$)

In general, *G*2 are mid-level and high-level clouds, which have lower opacity than *G*1 clouds. They attenuate direct solar radiation between 60% and 80%. There are different sky conditions that cause this attenuation levels, and two of those situations are shown in Fig. 1C and D. Fig. 1C shows cirrostratus (Cs) that covers large areas. Cs is generally thin, uniform and whitish, with some exceptions, when they are strip-shaped and extend across large parts of the sky. The sun can shine through Cs, and sometimes the sun will appear to have a clear halo (Fig. 1C). Another type of cloud formation that causes similar attenuations is altocumulus (Ac) which are small clouds with a cottony appearance, as the Ac translucidus shown in Fig. 1D. They are usually

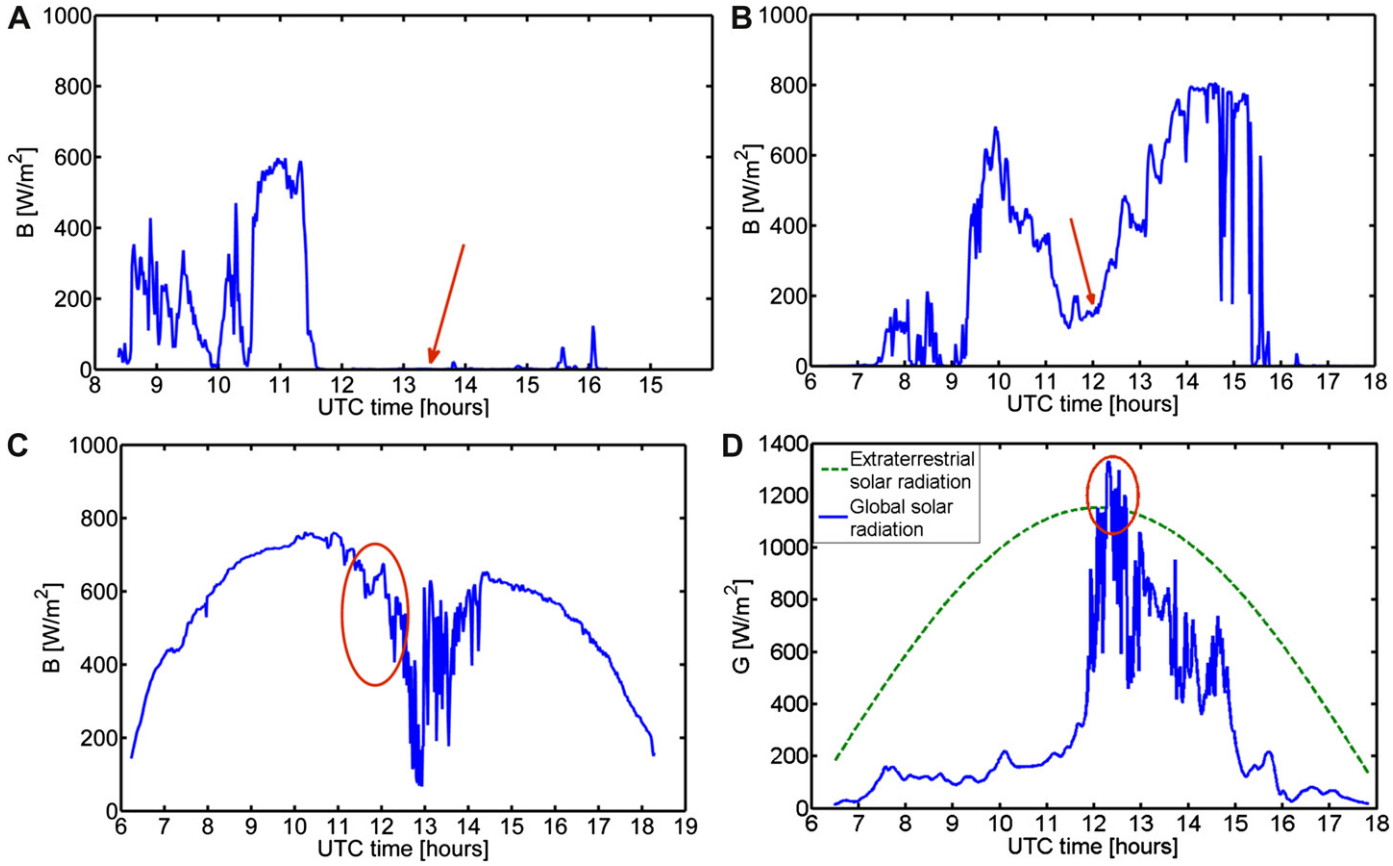

Fig. 2. Direct normal radiation corresponding to different clouds: (2A) G1, 2010/01/19; (2B) G2, 2010/04/22; (2C) G3, 2009/08/03; (2D) G4, 2010/04/17.

placed in groups characterised by globular masses with individual elements that are slightly smaller, less dark, and more ordered than other cloud types also included in this group, like the Cirrus (Ci) castellanus. Normally, these clouds are not welded together, leaving hollows through which blue sky can be seen. Additionally, these clouds are usually clear grey with slightly darker areas interspersed.

Fig. 2B shows the attenuation caused by the clouds seen in Fig. 1C. For approximately an hour, the direct solar radiation attenuation was strong, as the direct solar radiation was reduced to 200 W/m^2, although it was never completely attenuated.

4.1.3. Attenuation group 3, G3 ($0.4 < k_b < 0.6$)

*G*3 is normally made up of slightly opaque, usually thin, Ci clouds. A variety of different Ci belonging to this group has been found. An example of a sky situation with Cs that occurs in *G*3 can be seen in Fig. 1E. Cs clouds are thin and generally uniform and the sun can be seen through them. In certain occasions they are capable of forming halos. However, they are thick enough to be seen. Their colour is whitish, usually with no distinguishing features; their edges are not well defined, although some rounded edges can be appreciated, giving them a slightly "cottony" appearance. Normally, they do not cover the whole sky. Fig. 1F shows another type of Cs with possible presence of contrails. They are very thin and elongated blocking the sun's disk and producing mild attenuations. This type of cloud is often accompanied by tufts, and its colour is usually whitish.

Furthermore, the ellipse in Fig. 2C marks the effect of the cloudiness shown in Fig. 1E on the direct solar radiation. These clouds obstructed the solar disk for 1.5 h. During this period, direct radiation levels were reduced by up to 400 W/m^2. This period was then followed by more opaque clouds (observed near the northwest horizon in Fig. 1E), which attenuated more direct radiation.

4.1.4. Attenuation group 4, G4 ($k_b > 0.6$)

In this group, we found many cases in which there were no apparent clouds blocking the sun's disk, but the k_b value calculated clearly showed the effect produced by these thin clouds (normally Ci clouds, negligible to the naked eye).

Sometimes, clouds are too thin to be discernible, which is the case of Ci fibratus in the image shown in Fig. 1G. This type of clouds is characterised by poorly defined edges, and can be observed only when illuminated with direct or circumsolar radiation, which gives them a whitish colour. In addition, there have been some special situations in which, instead of attenuating solar radiation, certain clouds increased global radiation values to levels close to the extraterrestrial solar radiation. These clouds, as the As shown in Fig. 1H, are usually white broken clouds. They are situated near the solar disk, and their edges are well defined.

Finally, Fig. 2D shows the enhancement of solar radiation produced by the broken clouds in Fig. 1H. Unlike the other graphics, showing direct solar radiation, Fig. 2D shows global solar radiation and extraterrestrial solar radiation over a day. In the period pointed by the ellipse, the peak levels achieved by the global solar radiation matched the extraterrestrial solar irradiance value and even exceeded it. These radiation peaks could not be detected for higher acquisitions times (e.g., 1 h).

4.2. Cloud cover study for Almería

In this section, a thorough annual and seasonal analysis of cloud cover present in Almería is presented. First, we analysed the duration and the frequency of occurrence for the different types of sky situations during the studied period. Then, the proportions of the different sky conditions analysed in Section 4.1 are presented to

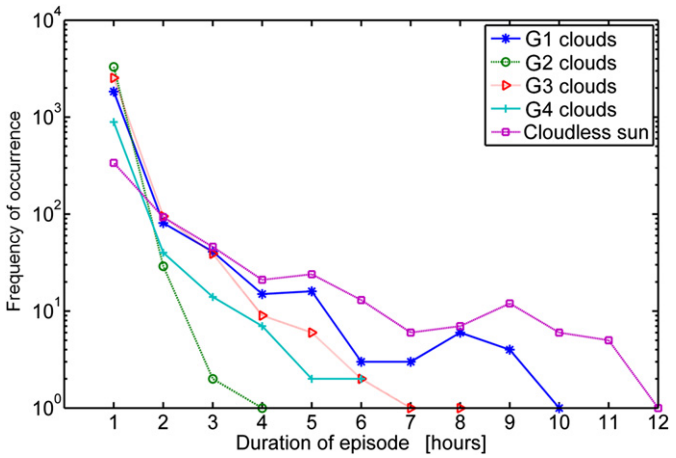

Fig. 3. Analysis of annual frequencies of cloud groups.

discern what direct solar radiation attenuations predominated at different times of the year in the studied area. This information is very interesting because knowing the distribution of the attenuation produced in direct solar radiation (and therefore the resulting radiation that reached the surface) throughout the seasons is necessary to exhaustively evaluate the available solar resource. To achieve this evaluation, we based this new study on the classification made in Section 3.2 on the k_b levels, which considered cloud types and not hidden sun events ("cloudless sun"). Consequently, these studies provided useful information for strategies in the use of renewable energy, particularly when employing solar energy in the area of interest.

A frequency analysis of *episode durations* (the time that the same cloud remains blocking the solar disk) for each group has been made. For completeness, cloudless sun episodes have also been included in this frequency analysis.

As Fig. 3 shows, all the different sky situations showed similar behaviours for episodes of one to 2 h, after which the duration of each sky situation was different. *G*2 episodes did not last more than 4 h, whereas episodes lasting more than 6 h were not found for *G*3 and *G*4 clouds. *G*1 clouds and *cloudless sun* were the longest events, with episodes lasting up to 9 and 12 h, respectively. As we found for the studied area, *G*1 clouds represented completely overcast conditions (see Fig. 1A and B) that occurred for many hours (i.e., when the sky is obscured). Furthermore, cloudless sun situations were the sky conditions with the longest duration throughout the studied period.

The presence of the different sky situations found in Almería was also analysed in this report. First, the proportion of each situation was studied on a seasonal basis, and they were then examined over the whole experimental period. Fig. 4 shows the resulting percentages of each group in the four seasons. A fifth sector represents the proportion of cloudless sun situations in the same time frame.

If we considered the presence of cloudless sun situations, a clear predominance could be detected in the spring and summer. Furthermore, this percentage of cloudlessness did not drop below 20% during the rest of the year. In contrast, G1 clouds (i.e., the most opaque clouds) were the most common group, at approximately 50% of the prevailing clouds in winter. With respect to the clouds included in *G*2 and *G*4, the ratio that they represented in each season was similar, at around 10%. Furthermore, *G*3 clouds behaved similarly throughout the year, representing approximately 20% of clouds in all-sky conditions, except in autumn, when they became the dominant cloud type at 31%.

Section 2 showed that Almería has significant seasonal variation in weather patterns. Spring and summer months are very dry with

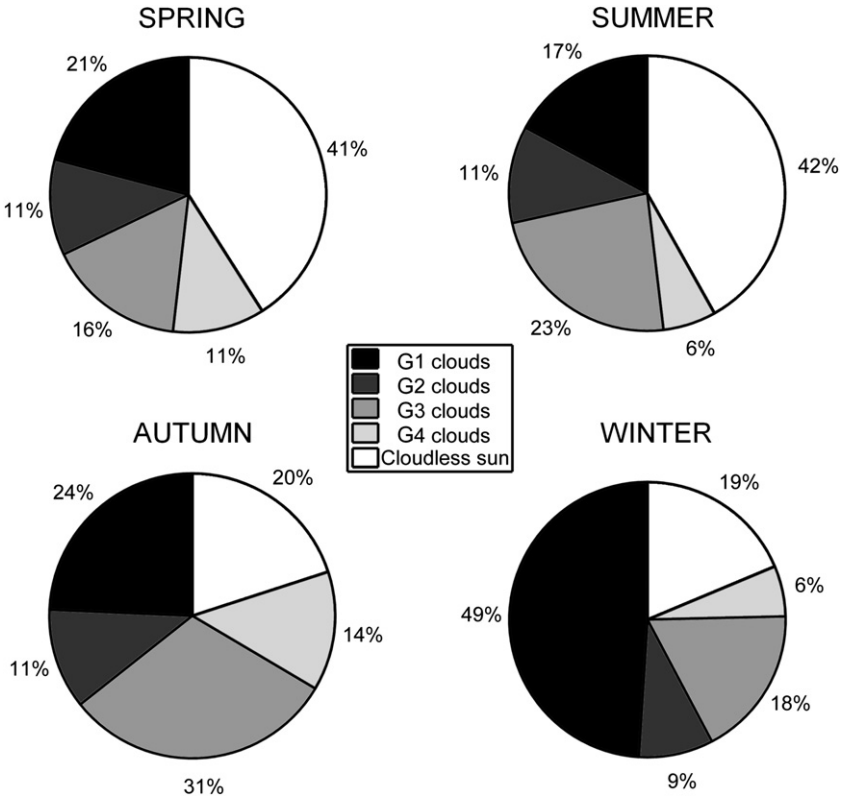

Fig. 4. Seasonal occurrence of different types of sky situations in winter, spring, summer and autumn.

Table 3
Annual occurrence of the sky conditions in Almería.

Attenuation Group	Frequency of occurrence (%)
G1	24
G2	11
G3	21
G4	9
Cloudless sun	35

little rainfall, thing which agrees with the prevalence of cloudless sun situations in these seasons; most of the annual rainfall occurs in winter and autumn. Accordingly, we can conclude that the months with the highest availability of solar resource were those of summer and spring.

Finally, the presence of the different sky situations in Almería was reviewed on an annual basis in this report. As such, Table 3 shows the percentages of each sky situation in the studied period.

There was a clear dominance of cloudless sun episodes over all the studied groups. Moreover, if we add the 9% corresponding to *G*4 clouds (which did not significantly attenuate direct solar radiation), we confirm that there are suitable weather conditions to exploit solar energy during over half of the year in the studied area. Specifically, the direct component of solar radiation reaching the surface, which is used by different solar energy generation systems, is high in this region. Additionally, the most opaque clouds (i.e., those that cause attenuation above 60% to direct solar radiation) represented 35% of the total cases (the sum of *G*1 and *G*2 cases).

Conversely, *G*2 and *G*4 clouds were the least frequent in the studied period, amounting each to approximately 10% in the whole dataset.

5. Conclusions

Due to the increasing demand for power generation using solar energy, a worldwide effort is being made to improve the solar resource assessment models. For this purpose, clouds must be considered and studied because of their main role as radiation attenuators. Therefore, both knowledge of the prevalence of each cloud system pattern and the attenuation caused by these clouds are of particular importance. In this study, we classified different sky conditions by their attenuation caused to the direct solar radiation at normal incidences. This attenuation was quantified according to the dimensionless index k_b, defined as the ratio of direct solar radiation to extraterrestrial solar radiation. To accomplish this assessment, radiation data and images from a TSI-880 were used.

One of the main conclusions from this work was that k_b was very representative of the attenuation caused by different clouds, allowing a characterisation of the cloud types obstructing the solar disk. This classification was then used to analyse the cloud cover over a Mediterranean location (Almería).

Different sky conditions were also studied in this work. As part of the analysis, the time that each sky condition lasted and its frequency of occurrence were measured; the occurrence of these sky conditions, both annually and seasonally, was calculated. From these studies, the following conclusions were drawn: According to the duration and frequency analysis, the most prolonged sky conditions in the studied area were the cloudless sun situations (i.e., the solar disk was not obstructed by clouds), with episodes lasting up to a whole day. These were followed by *G*1 cloud episodes with several episodes of almost 9 h. With respect to the occurrence of different sky conditions, a clear dominance of cloudless sun situations was found during the summer and spring, in more than 40% of the total sampled situations. Moreover, during the winter, *G*1 clouds were the most abundant, constituting nearly half of the studied situations for this season. The results thus showed a clear correlation with rainy and dry periods in this Mediterranean location (i.e., the months with the largest number of cloudless sun situations coincided with the driest periods in the studied area).

Knowledge of information regarding the cloud cover characteristics is very important to understand the behaviour of clouds in a particular area throughout the year. The performed analysis is particularly interesting when a comprehensive assessment of the available solar resource is conducted to determine the proper location of systems using solar energy, such as solar thermal plants. To this end, this study provides further details regarding the times during the year in which there will be more solar resource available for exploitation by different power production devices and it also offers valuable information in the regard of sizing the storage systems of a power plant. In future research, the use of satellite images and artificial intelligence techniques could lead to a more quantitative and comprehensive study of cloud cover that influences the availability of solar energy at a place.

Acknowledgements

The authors wish to acknowledge the Gemasolar Project, financed by Torresol Energy Investments, S.A.; the project ENE2007-67849-C02-02, financed by the Ministerio de Educación y Ciencia; and the grant financed by local government Junta de Andalucía. Authors are also grateful to Dr. Emilio Cuevas-Agulló (Agencia Estatal de Meteorología, AEMET) for his valuable comments and proofreading of this work.

References

[1] Fricker HW. Regenerative thermal storage in atmospheric air system solar power plants. Energy 2004;29:871–81.
[2] Lopez-Martinez M, Rubio FR. 2002. Cloud detection system for a solar power tower plant. IECON Proceedings (Industrial Electronics Conference); 3:2560–2565.
[3] Robaa SM. Evaluation of sunshine duration from cloud data in Egypt. Energy 2008;33:789–95.
[4] Sabziparvara AA, Shetaeeb H. Estimation of global solar radiation in arid and semi-arid. Energy 2007;32:649–55.
[5] Orsini A, Tomasi C, Calzolari F, Nardino M, Cacciari A, Georgiadis T. Cloud cover classification through simultaneous ground-based measurements of solar and infrared radiation. Atmos Res 2002;61:251–75.
[6] Dürr B, Philipona R. Automatic cloud amount detection by surface longwave downward radiation measurements. J Geophys Res-Atmos 2004;109:1–9.
[7] Schade NH, Macke A, Sandmann H, Stick C. Total and partial cloud amount detection during summer 2005 at Westerland (Sylt, Germany). Atmos Chem Phys 2009;4:1143–50.
[8] Zarzalejo LF, Ramirez L, Polo J. Artificial intelligence techniques applied to hourly global irradiance estimation from satellite-derived cloud index. Energy 2005;30:1685–97.
[9] Bosch JL, Batlles FJ, Zarzalejo LF, López G. Solar resources estimation combining digital terrain models and satellite images techniques. Renewable Energy 2010;35:2853–61.
[10] Derrien M, Farki B, Harang L, LeGléau H, Noyalet A, Pochic D, et al. Automatic cloud detection applied to NOAA-11 /AVHRR imagery. Remote Sens Environ 1993;46:246–67.
[11] Perez R, Ineichen P, Moore K, Kmiecik M, Chain C, George R, et al. A new operational model for satellite-derived irradiances: description and validation. Sol Energy 2002;73:307–17.
[12] Mefti A, Adane A, Bouroubi MY. Satellite approach based on cloud cover classification: estimation of hourly global solar radiation from meteosat images. Energ Convers Manage 2007;49:652–9.
[13] Calboć J, Pages D, Gonzaćlez JA. Empirical studies of cloud effects on UV radiation. A Review.Rev Geophys 2005;43:1–28.
[14] Alados-Arboledas L, Alados I, Foyo-Moreno I, Olmo FJ, Alcaćntara A. The influence of clouds on surface UV erythemal irradiance. Atmos Res 2003;66: 273–90.
[15] López ML, Palancar GG, Toselli BM. Effect of different types of clouds on surface UV-B and total solar irradiance at southern mid-latitudes: CMF determinations at Córdoba, Argentina. Atmos Environ 2009;43:3130–6.
[16] Pfister G, McKenzie RL, Liley JB, Thomas A, Forgan BW, Long CN. Cloud coverage based on all-sky imaging and its impact on surface solar irradiance. J Appl Meteorol 2003;42:1421–34.

[17] Sabburg JM, Long CN. Improved sky imaging for studies of enhanced UV irradiance. Atmos Chem Phys 2004;4:2543–52.
[18] Kassianov EI, Long CN, Ovtchinnikov M. Cloud sky cover versus cloud fraction: whole-sky simulations and observations. J Appl Meteorol 2005;44: 86–98.
[19] Long CN, Sabburg JM, Calbó J, Pagès D. Retrieving cloud characteristics from ground-based daytime color all-sky images. J Atmos Oceanic Technol 2006; 23:633–52.
[20] Estupiñán JG, Raman S, Crescenti GH, Streicher JJ, Barnard WF. Effects of clouds and haze on UV-B radiation. J Geophys Res-Atmos 1996;101: 16807–16.
[21] Tovar J, Olmo FJ, Batlles FJ, Alados-Arboledas L. Dependence of one-minute global irradiance probability density distributions on hourly irradiation. Energy 2001;26:659–68.
[22] Orgill JF, Holland KGT. Correlation equation for hourly diffuse radiation on a horizontal surface. Sol Energy 1977;19:357–9.
[23] Olmo FJ, Vida J, Foyo I, Castro-Diez Y, Alados-Arboledas L. Prediction of global irradiance on inclined surfaces from horizontal global irradiance. Energy 1999;24:689–704.
[24] Markou MT, Kambezidis HD, Bartzokas A, Katsoulis BD, Muneer T. Sky type classification in Central England during winter. Energy 2005; 30(1667):74.